Biomed Microdevices (2007) 9:123–134
DOI 10.1007/s10544-006-9005-7

Quantitative measurement and control of oxygen levels in microfluidic poly(dimethylsiloxane) bioreactors during cell culture

Geeta Mehta · Khamir Mehta · Dhruv Sud · Jonathan W. Song · Tommaso Bersano-Begey · Nobuyuki Futai · Yun Seok Heo · Mary-Ann Mycek · Jennifer J. Linderman · Shuichi Takayama

Published online: 12 December 2006

Abstract Microfluidic bioreactors fabricated from highly gas-permeable poly(dimethylsiloxane) (PDMS) materials have been observed, somewhat unexpectedly, to give rise to heterogeneous long term responses along the length of a perfused mammalian cell culture channel, reminiscent of physiologic tissue zonation that arises at least in part due to oxygen gradients. To develop a more quantitative understanding and enable better control of the physical-chemical mechanisms underlying cell biological events in such PDMS reactors, dissolved oxygen concentrations in the channel system were quantified in real time using fluorescence intensity and lifetime imaging of an oxygen sensitive dye, ruthenium tris(2,2'-dipyridyl) dichloride hexahydrate (RTDP). The data indicate that despite oxygen diffusion through PDMS, uptake of oxygen by cells inside the perfused PDMS microchannels induces an axial oxygen concentration gradient, with lower levels recorded in downstream regions. The oxygen concentration gradient generated by a balance of cellular uptake, convective transport by media flow, and permeation through PDMS in our devices ranged from 0.0003 (mg/l)/mm to 0.7 (mg/l)/mm. The existence of such steep gradients induced by cellular uptake can have important biological consequences. Results are consistent with our mathematical model and give insight into the conditions under which flux of oxygen through PDMS into the microchannels will or will not contribute significantly to oxygen delivery to cells and also provide a design tool to manipulate and control oxygen for cell culture and device engineering. The combination of computerized microfluidics, *in situ* oxygen sensing, and mathematical models opens new windows for microphysiologic studies utilizing oxygen gradients and low oxygen tensions.

Keywords Oxygen sensing · PDMS · Microbioreactor · Microfluidics · Fluorescence intensity · Fluorescence lifetime imaging microscopy (FLIM) · Oxygen gradients · Myoblast · Ruthenium tris(2,2'-dipyridyl) dichloride hexahydrate (RTDP)

Electronic Supplementary Material is available in the online version of this article at http://dx.doi.org/10.1007/s10544-006-9005-7.

G. Mehta · D. Sud · J. W. Song · T. Bersano-Begey · N. Futai · Y. S. Heo · M.-A. Mycek · J. J. Linderman (✉) · S. Takayama (✉)
Department of Biomedical Engineering, University of Michigan, Ann Arbor, MI 48108, USA
e-mail: takayama@umich.edu

K. Mehta · J. J. Linderman
Department of Chemical Engineering, University of Michigan, Ann Arbor, MI 48108, USA
e-mail: linderma@umich.edu

S. Takayama
Macromolecular Science and Engineering, University of Michigan, Ann Arbor, MI 48108, USA

M.-A. Mycek
Applied Physics Program, University of Michigan, Ann Arbor, MI 48108, USA

M.-A. Mycek
Comprehensive Cancer Center, University of Michigan, Ann Arbor, MI 48108, USA

1 Introduction

To study cells under simulated physiological microenvironments *ex vivo* (e.g. three-dimensional cell cultures and development of so-called "animals-on-a-chip") (Park and Shuler, 2003), it is necessary to develop tools to enable quantitative real-time control of microenvironment of cell culture in microbioreactors. This approach requires three main components: (i) the ability to *actuate* the spatio-temporal

distribution of nutrients, growth factors, and adhesive signals in the cellular microenvironments, (ii) the ability to *sense/measure* nutrients, metabolites, growth factors, cytokines, and other cell-secreted products, and (iii) the ability to quantitatively *model* the relationship between various design and operating parameters to enable control and operation of the bioreactor. Our previous studies with development of highly versatile computerized microfluidic bioreactor arrays (Gu et al., 2004) are hence still incomplete in that they lack integration of chemical sensors and quantitative understanding of the bioreactions involved through modeling. This paper specifically addresses these issues for a crucial cell substrate, oxygen, by developing an optics-based method to quantify dissolved oxygen in PDMS microbioreactors and by applying a quantitative mathematical model to explain how key parameters control the spatial distribution of oxygen inside them.

Oxygen is a very important nutrient for cell culture, and its lower solubility in culture media (less than 7 mg/L at 37°C) makes it imperative that it is constantly monitored and supplied (Fleischaker and Sinskey, 1981). One of the reasons PDMS microbioreactors are advantageous for cell-based studies is due to high diffusivity ($D = 4.1 \times 10^{-5}$ cm^2/sec) (Charati and Stern, 1998) and solubility (0.18 cm^3 (STP)/cm^3 atm) (Merkel et al., 2000) of oxygen in PDMS compared to other polymers and materials used for bioreactor and microfluidic device fabrication. Because of these properties of PDMS, passive permeation of oxygen through PDMS is generally assumed to be sufficient for supplying necessary amounts of oxygen for insect and mammalian cell cultures, which do not have very high oxygen uptake rates, and investigators do not typically quantify actual in-channel oxygen concentrations during microfluidic cell culture (Leclerc et al., 2003, 2004, 2006, Walker et al., 2002). Even within the range of oxygen concentrations sufficient for cell survival, the concentration of oxygen has a profound influence on cell signaling, growth factor production, growth, and differentiation (Muschler et al., 2004). Different types of cells require different oxygen concentrations for optimal physiological function. Human embryonic stem cells benefit from low oxygen concentration (below 5%) in order to maintain their pluripotency, and transient changes in oxygen levels can change gene transcription and affect fate of stem cells in culture conditions (Ezashi et al., 2005). Hematopoeitic stem cells (HSC) self-renew and maintain pluripotency better at lower oxygen tension (lower than 5% *in vitro*), and at higher oxygen levels *in vitro*, HSCs differentiate, and undergo apoptosis (Csete, 2005). Hence, there is considerable interest in the design of poly(dimethylsiloxane) (PDMS) microbioreactors conducive for culture of different types of cells, particularly cells requiring low oxygen tension.

There are various reports of measuring oxygen concentrations inside microfluidic devices using optical as well as polarographic measurements (Benninger et al., 2005; Chang-Yen and Gale, 2003; Mitrovski and Nuzzo, 2005; Park et al., 2006; Sin et al., 2004; Szita et al., 2005; Vollmer et al., 2005). Typically, electrode or fluorescence-based sensors are used to monitor dissolved oxygen content in cell cultures (Andreescu et al., 2004; Deshpande and Heinzle, 2004; Gerritsen et al., 1997; Helmlinger et al., 2000; Hwang et al., 2004; John et al., 2003; Malda et al., 2004; Sud et al., 2006b; Sweet et al., 2002; Tolosa et al., 2002; Urayama et al., 2003; Zhong et al., 2003). Polarographic oxygen sensors based on Clark electrodes have been widely used for monitoring oxygen in cell cultures. However, they suffer from disadvantages including: consumption of oxygen; long-term instability; sterilization problems; sensor drift; difficulty of adaptation to continuous monitoring, automation, and high-throughput measurement; flow dependence; and susceptibility to electrical interferences (Andreescu et al., 2004; Malda et al., 2004; Sweet et al., 2002). Most of these drawbacks are overcome by using optical oxygen sensors based on quenching of fluorescence by oxygen (Deshpande and Heinzle, 2004; Hwang et al., 2004; John et al., 2003; Tolosa et al., 2002). Fluorescence is attenuated in the presence of oxygen in a linearly dependent manner. Optical sensing is performed either through steady-state intensity based or lifetime based methods (Gerritsen et al., 1997; Sud et al., 2006b; Urayama et al., 2003; Zhong et al., 2003).

Previous efforts on modeling oxygen transport in microchannels have shown that the spatial distribution of oxygen concentration is a function of operating velocities and the channel geometry and significant gradients in oxygen concentrations can exist in the bioreactor especially at low flow rates (Mehta and Linderman, 2006; Roy et al., 2001). Theoretical studies of transport of oxygen have shown the possibility of axial concentration gradients in PDMS devices without any cells (Vollmer et al., 2005). Application of such mathematical models to real devices, however, requires validation with actual measurements. Some experimental studies have detected changes in oxygen concentration in a continuously perfused PDMS microbioreactor for cell culture (Park et al., 2006; Szita et al., 2005). While steep gradients (greater than 50% change in oxygen tension within 1 cm along the length of the bioreactor) have been observed in bacterial cultures in PDMS microbioreactors (Park et al., 2006; Szita et al., 2005; Zanzotto et al., 2004), no studies have reported such steep gradients in oxygen concentrations for mammalian cell culture in continuously perfused PDMS microbioreactors. Yet such steep gradients could clearly facilitate the function of those mammalian cells that need low oxygen tension, as in the studies of tissue zonation in perfused sinusoids due to oxygen gradients. When cells are cultured in a non-gas-permeable microbioreactor, it is well known that uptake by cells can reduce oxygen levels, leading to the formation of gradients of oxygen concentration

along the length of the cell culture channel (Allen and Bhatia, 2003; Allen et al., 2005). Native PDMS is highly oxygen permeable, but the permeability is subject to change when proteins are adsorbed on it or when the surface is modified by plasma oxidation as is common in construction of microbioreactors (Shiku et al., 2006). Shiku et al. (2006) demonstrated that the mass-transfer coefficient of oxygen through PDMS is reduced 1000-fold after a 5 min plasma oxidation, and reduced by 5 times after 20 min incubation with bovine serum albumin. Furthermore, the use of parylene C coating in the PDMS devices can add additional diffusive resistance to the oxygen transfer from the ambient air owing to the lowered permeability of the composite layer. Thus, it is crucial to confirm theoretical models with experimental measures for each type of device where the plasma oxidation conditions, protein coating methods, and other culture device fabrication and preparation methods vary, even when the devices are all made of "PDMS". Indeed, oxygen gradients in PDMS microbioreactors may be significantly steeper than expected if the oxygen permeability of device material is low.

Here, we quantitatively measure extracellular oxygen concentration in the microfluidic channels inside PDMS bioreactors containing living cells by using fluorescence intensity and lifetime studies. Fluorescence lifetime imaging microscopy (FLIM) bases image contrast on lifetime variations, which reflect local biochemistry but are oblivious of intensity based artifacts such as scattering, photobleaching and concentration variation of fluorophore. Calibration of ruthenium tris(2,2'-dipyridyl) dichloride hexahydrate (RTDP) lifetime on a wide-field, time domain FLIM system was employed to calculate dissolved oxygen concentrations via fluorescence intensity studies (Sud et al., 2006a; Sud et al., 2006b; Urayama et al., 2003; Zhong et al., 2003). Optical sensors for oxygen estimation are beneficial since they are suited for small volumes, are minimally perturbing, and do not consume oxygen during the measurement. This technique may be used for time-lapse studies (hours or days) without disturbing the set-up, and for imaging of spatial oxygen distributions.

Using a mathematical model we have previously shown that the concentration of soluble nutrients can be manipulated by controlling operating conditions and by using channels of appropriate geometry (Mehta and Linderman, 2006). We utilize this mathematical model that describes oxygen diffusion, convection, and uptake by cells within the device to draw comparisons between the model and the experimental results, and to determine the contribution of oxygen flux through PDMS to overall oxygen delivery to cells.

In this work, we show that by manipulating the operating variables, e.g. media flow rates, one can effectively achieve the desired oxygen tensions inside the bioreactor. We also see that the relative supply of oxygen via diffusion through PDMS can also be altered using the media flow, as per the model predictions. Additionally, we show that oxygen diffusion through PDMS is not always sufficient to avoid oxygen concentration gradients along the length of the bioreactor even in culture of mammalian cells that have much lower oxygen uptake rates compared to bacterial cells. The validation of the model predictions also enables its use in controlling the oxygen levels inside the reactor. This combined capability to experimentally measure in-channel oxygen concentration gradient and to fit device-specific parameters to mathematical models ultimately propels us towards our goal of producing well-defined and controlled oxygen tensions inside PDMS microbioreactors.

2 Materials and methods

2.1 Cell culture

C2C12 cells (mouse myoblasts, ATCC, CRL–1772) were cultured in a media comprising Dulbecco's Modified Eagle's Medium (DMEM, 11960, Gibco), 15% Fetal bovine serum (FBS, 10082, Gibco), 1%v/v antibiotic–antimicotic (15240, Gibco) and 1%v/v GlutaMAX2-I Supplement (35050, Gibco). The 100 mm^2 culture dishes were placed in a humidified 5% CO2 cell culture incubator. At 70–80 % confluence, the cells were passaged by washing in PBS, and incubating with 0.25% Trypsin/EDTA (Invitrogen, Carlsbad, CA). The Trypsin solution was neutralized with 15% FBS in DMEM and spun down with a centrifuge (ThermoForma, Marietta, OH) for 2 min at 25°C and 1000 RPM. The supernatant was removed and the pellet was resuspended in DMEM media. The pellet was reconstituted in 4 ml of DMEM media, and 1 ml of this suspension was used for creating a new plate of C2C12. The cells were passaged every third day. When the cells were to be cultured in the PDMS microbioreactor, the pellet was reconstituted in 70–100 μL of DMEM media and then injected into the seeding ports of the chip.

2.2 Preparation of the microfluidic bioreactor chip

The chip consisted of three components: reservoir top layer, channel middle layer and membrane bottom layer, as seen in Fig. 1(A). The chips were formed from pre-polymer (Sylgard 184, Dow Corning) at a ratio of 1:10 base to curing agent. The top layer contained fluid reservoirs and was cured overnight at 60°C. The middle layer was formed using a glass wafer mold (soft lithography) (Duffy et al., 1998) to form a layer with negative relief channel features $\sim$30 μm in height and 300 μm in width. The positive relief features of the mold were composed of SU-8 (Microchem, Newton, MA) formed on a thin glass slide (200 μm thick) using backside

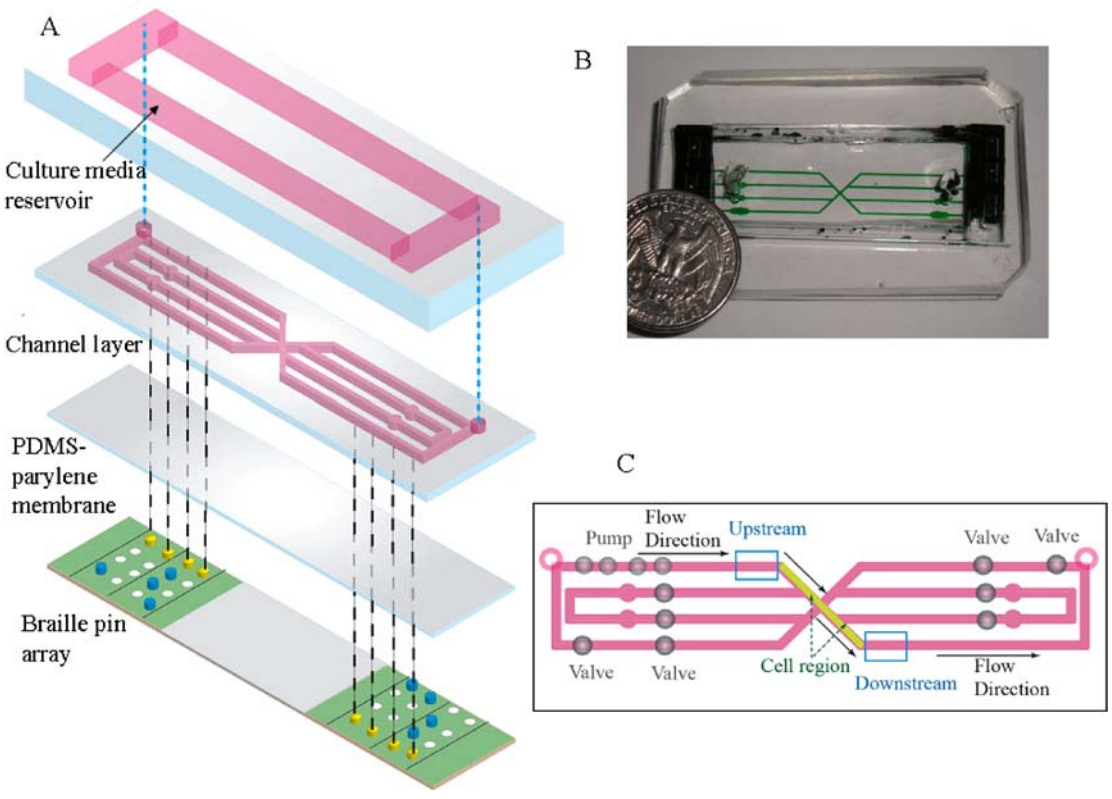

Fig. 1 Microfluidic device design and set up. (A) The top layer of the microfluidic device is a reservoir layer, connected to the channel layer with punched holes (pink holes in channel layer connected to the reservoir layer with a dashed blue line). A "horizontal" pump (yellow pins) drives cell culture media from top left to bottom right, all other channels are valved closed (blue pins are raised to close channels by deformation), and rest of the pins are in valve open position (white pins are down). The cells are attached in a part of the X-shaped channel region, between top left and bottom right. (B) Optical photomicrograph of a complete device with green food dye to showcase channel design, placed with a quarter for scale. (C) Top view of channel layer showing the positions of the pin driven pumps and valves when the device is used for continuous perfusion experiments. The flow direction (black arrows), areas of cell growth (green with green arrows), and, upstream and downstream positions (blue rectangles) where images were taken are shown in the figure. The flow in some of the channels is stopped by valves (grey with dark black borders), while flow is allowed in the desired channels by use of pumps (grey with no border)

diffused-light photolithography (Futai et al., 2004). The glass slide was silanized with tridecafluoro-(1,1,2,2-tetrahydrooctyl)-1-trichlorosilane (United Chemical Technologies Inc., Bristol, PA). The middle layer was also cured overnight at 60°C and holes were punched (Dermal biopsy puncher, Miltex Inc., York, PA) in the channel and reservoir layer to connect channel features to the culture media reservoir. The thickness of PDMS above the channel feature was 6 ± 2 mm. The bottom layer was a thin sandwich of PDMS (100 μm)-parylene C (2.5 μm)-PDMS (100 μm) prepared by spin coating (Cee 100 Spin Coater, Brewer Science Inc., Rolla, MO) PDMS and vapor deposition of parylene C (PDS 2010 labcoater; Specialty Coating Systems) and curing PDMS at each step in an oven at 60°C overnight (Heo et al., 2006). The hybrid membrane was oxidized in oxygen plasma (SPI Supplies, West Chester, PA) for 30 s thereby making the PDMS surfaces hydrophilic. The layers were sealed irreversibly, the flat surfaces were pressed together, and the entire chip was placed in an oven at 60°C for 5–10 min. The oxygen permeability (a crucial transport property which incorporates diffusivity and solubility) of parylene C is 3.24×10^{-10} (cm^3 (STP) cm)/(cm^2 sec atm) (Yeh et al., 1990), while that of PDMS is $6.0800 \pm 0.1519 \times 10^{-6}$ (cm^3 (STP) cm)/(cm^2 sec atm) (Merkel et al., 2000). The bottom hybrid membrane hence has lower oxygen permeability due to the parylene layer, despite being much thinner ($\sim$8 mm PDMS vs 0.2 mm PDMS plus 0.0025 mm parylene) than the upper all-PDMS layer. Such low diffusivity and solubility of the parylene layer hence ensures that there is minimal diffusion of oxygen from the bottom layer of the device.

Fibronectin (100 mg/μl, F2006, Sigma) was injected (30-gauge hypodermic needles) in the cell culture channels to maintain the hydrophilic nature of the channels and to promote cell attachment (see Fig. S1) http://dx.doi.org/10.1007/s10544-006-9005-7.. This absorption was carried out for 30 min, following which DI water was introduced. The chips were then sterilized by placing under UV light for $\sim$30 min. After sterilization, water was

replaced with DMEM media in the reservoir, and the chip was placed on an array of pin actuators adapted from Braille displays for at least one hour to peristaltically pump fluid through the channels (Futai et al., 2006; Heo et al., 2006; Song et al., 2005). C2C12 cells were then seeded into the chip. We were able to manipulate the cells to attach only in the area of the bioreactor in between the upstream and downstream channel regions by use of valves (pin actuators pushing up and deforming channels closed) during cell seeding (see Fig. S2). The cells were given 1–2 h to attach under no flow (pins up and channels valved closed) condition in a dry heat incubator (Forma 310 Series Direct Heat CO2 Incubator, Thermo electron Corporation**,** Marietta, OH) maintained at 37°C and 5% CO_2. Pumping was started after cells became adherent and the chip was perfused for 12–14 h. 0.2 ml of the oxygen sensitive dye, ruthenium tris(2,2'-dipyridyl) dichloride hexahydrate (RTDP) (93307, Fluka) (5 mg/ml in DPBS (14190250, Invitrogen); final concentration is 1 mg/ml because of dilution) was then introduced into the reservoir of the chip, and pumping was continued for three more hours. The setup comprised of a microfluidic chip attached to the pin actuator array module was then taken to the microscope and intensity or lifetime measurements were performed at room temperature. Cell densities in the cell culture channels in the microbioreactor chips were determined by counting the number of cells present in 10 microscope brightfield images taken at different positions along the length of the cell culture channel.

2.3 Fluid actuation

An array of 48 pin actuators adapted from a Braille display module (SC9, KGS, Saitama, Japan) was used for fluid actuation (Futai et al., 2006). The pin actuator module was controlled with a computer via Universal Serial Bus (USB) through a finger-sized stand alone custom controller circuit board (Olimex, Plovdiv, Bulgaria) (Futai et al., 2006; Heo et al., 2006). The microfluidic bioreactor chip interfaces with the pin actuator module by simply holding the chip in place such that the channels align with the pins which push upward closing the channel, as seen in Fig. 1(A) and (C).

The pin movements for valving and pumping were controlled with a custom computer program written in C #. The software program provides effective control of the Braille hardware setup and is flexible, enabling one to define new behaviors of pumping, blocking or opening channel paths, and controlling timing and flow rates for short and long-term automated control of microfluidic devices. This software can run on PCs and control specific custom Braille hardware through a USB connection, and it acts as an interpreter enabling us to write complex sequences of actions in a shorthand text form. Multiple threads of execution within the program handle the exact timing and order of events within a main execution loop. The shorthand description form allows us to create any number of pumps (3–4 Braille pins) and valves (1 Braille pin) on the 'grid' of braille pins (up to 16 columns and 4 rows for our setup, see Fig. 1(A)). We specify the position for each of the pumps or valves (which will have a different effect on flow depending on the overlayed channel design), and in the case of pumps also their alignment (horizontal or vertical), direction of pumping flow (positive or negative), and relative speed. We also specify time intervals on an execution time axis for each of these objects, which allows us to describe more complex sequences of events, e.g. pump1 starts at 0 s and stops at 30 s, then valve2 closes from 30 s to 50 s, and pump3 and pump1 turn on from 31 to 40 s. Fig. 1(C) shows the valves and pumps used for the continuous perfusion experiment. The software also has a user interface that allows starting, pausing, stopping, and even rewinding the execution of any loaded shorthand program of pumps and valves, and also has an independent speed control that allows running essentially the same program and sequence of actions but with different flow rates and faster or slower execution.

The average flow rate was controlled by changing the time delay between pin motions. Fluid flow was characterized by tracking 6 μm diameter fluorescent beads (Carnine, polystyrene microspheres, Molecular Probes, Eugene, OR) using a digital CCD camera (Orca-ER, Hamamatsu Photonics, Japan) and a fluorescence stereomicroscope (Nikon SMZ1500). The image sequences were acquired at $\sim$13 frames/sec to determine the velocity of the microspheres, which are representative of the fluid velocity, and were used to determine the average fluid flow rate. An entire pumping cycle was used to measure each flow rate in order to compensate for backflow during certain steps of a pumping cycle. The average flow rates used for these experiments were in the range of 0.0005 μl/sec to 0.22 μl/sec, and the flow rates were relatively linear with frequency. This was observed from the motion of polystyrene microspheres, and is outlined in Table 1.

Table 1 Average flow rates at different pumping time delays

Pumping frequency (Hz)	Average flow rate ($\times 10^3$ μl/sec)
0.01	0.50 ± 0.02
0.02	1.40 ± 0.40
0.04	3.00 ± 1.00
0.10	6.00 ± 2.00
0.20	12.4 ± 4.00
1.00	83.0 ± 23.0
5.00	220 ± 30.0

2.4 Fluorescence measurements

We used a Nikon TS100-F inverted microscope with Epi-Fluorescence using a 10x CFI Achromat ADL Ph1 objective (n.a. 0.25, w.d. 6.20 mm), TRITC HY-Q Filter Cube, and an X-CITE 120 PC Fluor illumination system to measure intensity of the RTDP dye in the microbioreactor. The pictures were recorded using the Coolsnap CF2 12 bit Firewire Monochrome Camera with MetaVue Software. Intensity measurements were taken at upstream and downstream locations of the perfused microbioreactor at different flow rates, and at different cell densities. The fluorescent images were taken at an exposure time of 0.6 s for each observation, and each area was sampled three times. In total, six data-sets were created by repeating the experiments at all flow rates. The relationship between fluorescence intensity (or lifetime) and dissolved oxygen concentration is described by the Stern-Volmer equation (Gerritsen et al., 1997; Sud et al., 2006b; Urayama et al., 2003; Zhong et al., 2003): $I_o/I = 1 + K_q[O_2]$ or $\tau_o/\tau = 1 + K_q[O_2]$, where I_o or τ_o = uninhibited sensor dye intensity or lifetime (i.e. 0% oxygen), I or τ = sensor dye intensity or lifetime at oxygen level $[O_2]$ and K_q is the Stern-Volmer quenching constant

For fluorescence lifetime studies, a time-domain FLIM system with a tunable, pulsed excitation source covering the UV-vis-NIR spectrum (337–960 nm) and an intensified, gated (min. 200 ps) CCD camera (Picostar, LaVision) to record images was used (Urayama et al., 2003). Lifetimes could be measured in the range of 750 ps—∞ with a discrimination of 50 ps, and an axial resolution of 1.4 μm. RTDP fluorescence from microbioreactor compartments were collected at 600 nm via 460 nm excitation at gates of 40, 140, 240, 340, and 440 ns, with the intensifier gate width set to 100 ns. A lifetime macro implementing the rapid lifetime determination (RLD) algorithm was used to generate lifetime images on a per pixel basis from gated intensity images (Urayama et al., 2003; Zhong et al., 2003). Oxygen levels were ascertained by fitting the Stern-Volmer equation to calculated lifetimes. The data were analyzed statistically by ANOVA, Tukey's test and Student's t test at a 95 percent confidence level assuming unequal variances.

2.5 Mathematical modeling

We adapted our previously published model of transport of soluble nutrient/growth factors inside a microchannel bioreactor for the current study (Mehta and Linderman, 2006). Briefly, partial differential equations were written to describe the spatial distribution of oxygen inside the bioreactor in the presence of the convective transport associated with media flow, diffusive flux through PDMS, and cellular consumption and were solved using FEMLAB®. We used a steady state model with constant cell density, as the experimental time scales are small compared to the doubling times of cells. The model assumes uniformly distributed cell density along the bioreactor, which is reasonable as the cells are seeded using a suspension, and as visualized from microscope images. We also assume that the cells are adherent to the channel walls and are preferentially located at the bottom floor of the channel. Further, the model assumes a laminar flow profile, Michaelis-Menten rate of uptake of oxygen by all cells, and a constant overall mass-transfer coefficient to describe the flux of oxygen through PDMS. We assume there is no flux of oxygen from the bottom because the thin bottom membrane contains a parylene film which has low diffusivity and permeability to oxygen relative to PDMS, as described in the preparation of the microfluidic bioreactor chip in the methods section and because we also placed a glass cover slide underneath this membrane in the cell observation region (flux from the top of the bioreactor is much more than that from bottom for modeling purposes). A brief description of model equations, geometry and the associated variables is shown in Fig. 2.

Analysis of the model equations in dimensionless form gives us information on the three key dimensionless groups important in determining the concentration distribution of oxygen inside the bioreactor: $Pe/\alpha = \langle u\rangle H^2/(D_e L)$; $Da = V_{max} \text{ø} H/D_e c_{in}$; $Sh = k_{la} H/D_e$. The dimensionless group Pe signifies the Peclet number ($Pe = \langle u\rangle H/D_e$), the ratio of convective transfer of species in the axial direction to the diffusive flux within the channel directed toward the lower end of the channel (i.e. toward the cell domain); α is the geometric aspect ratio for the bioreactor, L/H. The Damkohler number (Da) is a measure of relative rates of total cellular uptake and diffusive flux from the bulk media. The magnitude of diffusive flux from PDMS is governed by the value of the Sherwood number (Sh), defined as the ratio of the diffusive transfer rate through the PDMS top surface to the diffusion rate in the media.

Key parameters of the model include the Michaelis-Menten uptake rate parameters (V_{max} and K_m) and the overall mass transfer coefficient (k_{la}). For the current study, the these parameters were estimated from a single data set from our microbioreactor (corresponding to the cell density of 5.1×10^8 cells/m^2), with initial estimates based on physiologically relevant values (Allen and Bhatia, 2003) and then used to compare the model predictions with the remaining data. Calculations were made for several values of k_{la} for comparison with the experimental data.

3 Results and discussion

3.1 Device description

Figure 1(A)–(C) show the design and set up of the microfluidic bioreactor chip and its alignment with the pin actuator

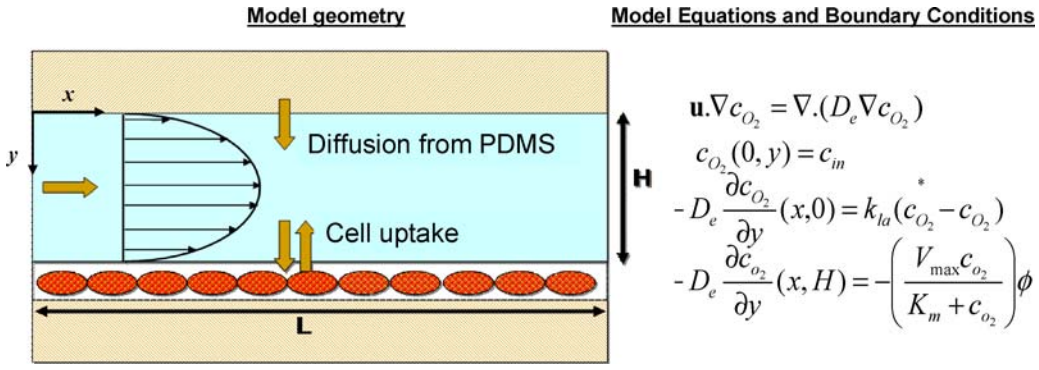

Fig. 2 Modeling oxygen transport in the microfluidic channel bioreactor. Assuming constant cell density and idealized rectangular geometry with cells preferentially located at the channel bottom, oxygen transport can be modeled using the partial differential equations shown. The boundary conditions in the y dimension are given by diffusive flux from PDMS at the top ($y = 0$) and by cellular uptake at bottom ($y = H$). The diffusive flux from PDMS can be estimated using an overall mass transfer coefficient k_{la} based on the solubility and diffusivity of oxygen in PDMS, while the uptake of oxygen by the cells is modeled as Michaelis-Menten kinetics with parameters V_{max} and K_m. Refer to Mehta & Linderman (2006) for further details on solution techniques and parameters. c_{o_2} : oxygen concentration, u : velocity profile, D_e : effective diffusivity of oxygen in the media ($= 2.1 \times 10^{-9}$ m^2/s), H : height of the microchannel (40 μm), L : length of the microchannel (0.01 m), ø : cell density, and velocity profile $\mathbf{u} = 6\langle u \rangle$ (y/H- (y/H)^2) where $\langle u \rangle$ is the average velocity

module (Futai et al., 2006). Three pin actuators act as a peristaltic pump pushing cell culture media through the microfluidic channels. The cells are seeded only in the area between the top left to bottom right of the X-shaped channel crossing region (shaded green in Fig. 1(C)). The bottom layer of the microfluidic bioreactor chip is a thin flexible membrane composed of PDMS and parylene C and has low oxygen permeability. During cell culture, the media is perfused (flow direction shown with black arrows in Fig. 1(C)) from top left to bottom right of the microbioreactor chip by pin actuators acting as pumps (yellow pins shown in Fig. 1(A), while all other channels are valved-off (blue raised pins). Within the parameters of the current experiments, this microfluidic bioreactor is a flow-through, rather than a recirculating, perfusion system. A part of the device (the X-shaped channel region) is viewable on an inverted microscope.

3.2 Local oxygen content measured by fluorescence intensity

We used different concentrations of the RTDP (in PBS) ranging from 0.1 mg/ml to 1.0 mg/ml, and found that dye signal was best at 1.0 mg/ml for both intensity and lifetime-based fluorescent imaging. Thereafter, 1.0 mg/ml of RTDP in culture media was used for all cell experiments. RTDP quenching by oxygen is a collisional process described by the Stern-Volmer equation. We employed $K_q = 2.7 \times 10^{-3}$ μM^{-1} for our measurements, as reported (Gerritsen et al., 1997) and verified via FLIM (Sud et al., 2006a,b).

Our negative control comprised of microfluidic chips containing only DMEM media and RTDP and no cells. We used the intensity and lifetime observed in this control device for calculating the intensity at zero oxygen content. We observed that the average intensity of RTDP over different flow rates at upstream and downstream positions was 327 $\pm$ 7 AU, while, the average RTDP lifetime over different flow rates at upstream and downstream positions was 307 $\pm$ 7 ns. This corresponds to 8.2 mg/l of dissolved oxygen in media in the microbioreactor in the absence of any cells, while the saturation dissolved oxygen content in an aqueous solution is 8.5 mg/l at 25°C (Fleischaker and Sinskey, 1981). Thus, intensity at no oxygen was calculated using the Stern-Volmer equation, and found to be 550 AU. The Stern-Volmer equation describes the relationship between ($I/I_o - 1$) and dissolved oxygen to be linear, as was seen in our calibration (data not shown). Thus, the intensity values obtained from the microbioreactor culture could be translated into local dissolved oxygen levels.

3.3 Observed oxygen gradients are a function of flow rate and cell density

We measured oxygen concentration at the upstream and downstream regions of the cell culture channel (see Fig. 1(C)) in our perfused bioreactor culturing C2C12 cells and found gradients that depend on both cell density and flow rate. The distance between each observation point and cell culture region was essentially the same. The relationship between flow rate and oxygen content at six cell densities, ranging from 1.92×10^8 cells/m^2 to 8.01×10^8 cells/m^2, is depicted in Fig. 3. The figure shows the upstream and downstream oxygen content for all cell densities and at seven different flow rates, ranging from 0.0005 μl/sec to 0.22 μl/sec.

Upstream oxygen concentrations remained steady at 8.2 $\pm$ 0.2 mg/l (corresponding to an oxygen partial pressure of 154 mm Hg, 20.7 % oxygen in air, or 97 % saturation) for

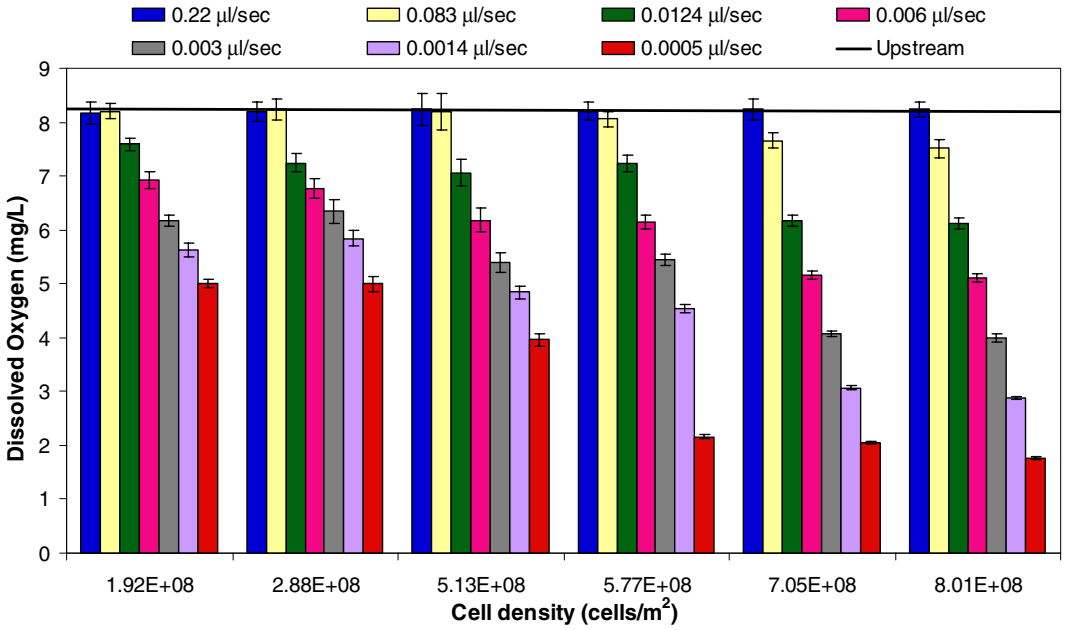

Fig. 3 Upstream and downstream extracellular oxygen in the microbioreactor at different flow rates and cell densities. The horizontal line depicts the upstream oxygen content of 8.20 ± 0.20 mg/L. The downstream oxygen concentrations are shown as a function of six different cell densities (from 1.92 × 10^8 cells/m^2 to 8.01 × 10^8 cells/m^2) at each at seven different flow rates, from fastest flow rate (0. 22 μl/sec) to slowest (0.0005 μl/sec)

all flow rates. Downstream oxygen concentrations varied with cell density and flow rate. The lowest value of dissolved oxygen content observed was 1.76 mg/L, which corresponds to the lowest flow rate of 0.5 nL/sec and the highest cell density (8.01 × 10^8 cells/m^2) tested. In contrast, the downstream dissolved oxygen content observed at low cell densities and the highest flow rates was nearly identical to the upstream concentration.

As shown in Fig. 3 for each cell density, as the flow rate decreased the difference between upstream and downstream dissolved oxygen content increased. The concentration of oxygen decreases down the cell culture channel axis because the cells present along the axis consume oxygen. At slower flow rates the amount of oxygen-laden media coming into the culture channel is smaller, leading to a steeper concentration gradient. We also observed that for a constant flow rate, increasing cell density inside the culture channel caused oxygen content to decrease measured at the downstream region (Fig. 3).

The downstream (see Fig. 1(C)) oxygen levels at each flow rate (corresponding to a particular cell density) were statistically different from one another with a p value of less than 0.0001 (ANOVA). When comparing downstream oxygen tension data at each flow rate (at a particular cell density) with all other datasets using Tukey's test, differences were found to be statistically significant ($\alpha = 0.05$) for all comparisons. The downstream oxygen levels at each cell density (corresponding to a particular flow rate) were statistically different from one another with a p value of less than 0.0001 (ANOVA). When comparing downstream oxygen tension data at each cell density (at a particular flow rate) with all other datasets using Tukey's test, differences were also found to be statistically significant at $\alpha = 0.05$. The oxygen concentration values observed at different flow rates as well as different cell densities were statistically significant (t-test, $p < 0.01$) between the upstream and downstream regions (see Fig. 1(C)) of the cell culture channel. Comparison of the upstream oxygen tensions with those downstream for all cell densities and flow rates, using ANOVA gave p value of 0.024, which is statistically significant at $\alpha = 0.05$.

The oxygen tensions observed here are similar to those seen by Allen and Bhatia 2003) with hepatocyte culture in a perfused polycarbonate microbioreactor. They observed oxygen partial pressure differences of 23 to 133 mm Hg (1.2 to 7.1 mg/l) between the inlet and outlet of when perfusing a 55 mm long polycarbonate microbioreactor at flow rate of 0.4 ml/min to 3.0 ml/min (inlet pressure: 158 mm Hg), suggesting that there are axial gradients (0–0.107 (mg/l) mm) of oxygen within their device.

Oxygen gradients have been observed in physiological systems (Tsai et al., 2003). In microcirculation, there are radial and longitudinal gradients as oxygen exits through the vessel walls, which are related to the level of metabolic activity of the tissue. *In vivo* oxygen tensions range from 20 mm Hg to 100 mm Hg (1–8 mg/L in vessels of diameters of 20–300 microns) in different parts of the tissues of animal models (Duling, 1972; Pittman and Duling, 1975;

Seiyama et al., 1996; Swain and Pittman, 1989; Tsai et al., 2003). Thus, the downstream oxygen levels observed in our microbioreactor are comparable to physiological values for mammalian cells.

We used a high concentration (1 mg/ml) of RTDP to get good fluorescence signals at low exposure times. However, there are some studies suggesting that RTDP might have cytotoxic as well as phototoxic effects on mammalian cells (Dobrucki, 2001). For the scope of this study we confirmed that the presence of dye in the media contributed minimally (less than 10%) to cell death within the timeframe of the oxygen concentration measurement period (up to 5 h after dye injection) and the photoexcitation and measurements were performed in regions on the microfluidic bioreactor where cells were not present to avoid phototoxic damage to cells. We did observe that when cells were incubated with RTDP over long periods of time (24–72 h) their viability decreased with time. The actual rate of oxygen consumption without added RTDP may thus be higher than what we measured since any toxicity would most likely reduce respiration.

The presence of a gradient is not necessarily indicative of insufficient oxygen transport to the cells. But it is crucial to understand and characterize the gradients generated to be able to understand and regulate cellular responses in microfluidic bioreactors. The ability to generate and regulate oxygen concentration gradients may actually be beneficial for recreating physiologic gradients as is observed, for example, in liver sinusoids (Tsai et al., 2003). We note that steep oxygen gradients of the type we describe (up to 79% decrease in oxygen tension within 1 cm along the length of the bioreactor) have not previously been demonstrated for mammalian cultures in continuously perfused PDMS microdevices.

Our finding of a significant oxygen gradient may provide one plausible explanation for the gradient of cell proliferation previously observed in PDMS perfusion reactors (Futai et al., 2006; Gu et al., 2004). Specifically, they observed higher cell densities of cells at the inlet of the device relative to the regions near the exit, presumably in response to a nutrient concentration gradient along the length of the channel. The range of oxygen concentrations we observed is within a range where no adverse effects on viability or marked differences in differentiation patterns is expected for C2C12 cells, as under *in vitro* culture at low oxygen tensions (5 % oxygen or 2.0 mg/L) the C2C12 cells are at similar stages of differentiation (from myoblasts to myotubes) during the hypoxic and normoxic (21% oxygen) exposure periods (Yun et al., 2005). However, the C2C12 cells may have migrated upstream or otherwise functioned differently along the length of the perfusion channel (Gu et al., 2004) because the cells were exposed to a relatively steep gradient of oxygen concentration.

3.4 The experimental data are consistent with the mathematical model

The observed trends in the experimental data are consistent with the results of our mathematical modeling. Figure 4(A) shows the comparison of model predictions and experimental data on downstream oxygen concentrations for media flow rates and cell densities tested. The agreement between model and experiment suggests that the model captures the essential transport processes occurring in the microfluidic bioreactor. Analysis of model equations shows that when velocity is decreased relative to diffusion (low Pe/α) and for higher rates of uptake of oxygen inside the microfluidic cell cultures (high Da), the outlet concentration of oxygen decreases.

The model predicts generation of oxygen concentration gradient within PDMS channels. The relative magnitude of diffusion and convective transport are characterized by the overall mass-transfer coefficient and the media velocity in the model, and we use the model to investigate the relative contribution of diffusion through PDMS for various geometries and thicknesses of PDMS layers by varying the numerical value of the mass-transfer coefficient k_{la}.

We observed the effect of changing the overall mass-transfer co-efficient on the outlet concentration of oxygen in the microbioreactor (Fig. 4(B)). At low flow rates, higher values of k_{la} (higher Sh) lead to higher values of the oxygen concentration at the outlet. At these low flow rates, oxygen delivery to cells via diffusion through PDMS is a significant source of oxygen. It should be noted that at high flow rates, oxygen delivery occurs primarily via perfusion and is sufficient to eliminate axial gradients in the cell culture channel, and hence the value of k_{la} (Sh) does not affect the concentration of oxygen at outlet. Our data is best fit by a $k_{\mathrm{la}} = 9 \times 10^{-7}$ m/s. Our value of the mass-transfer co-efficient is lower than that mentioned by other researchers (e.g $\sim 10^{-4}$ m/s, Vollmer et al., 2005). The reduced oxygen permeability of our device is likely due to various coatings and pre-treatments, i.e. plasma oxidation and protein coating.

Using the measured experimental data from oxygen concentration at the outlet, we can estimate the cellular uptake rates of oxygen. This opens up the possibility of using these microfluidic bioreactors for quantitative evaluation of cell properties. However, we note that for successful parameter inference we will require more experimental data to cover a wider range of oxygen concentrations. For example, we could not see a sensitivity of model predictions on the uptake parameter K_{m} for the current experimental data, as most of the experiments were performed at concentrations of oxygen well above K_{m}. Nevertheless, using similar experimental protocols, and careful experimentation coupled with the mathematical model, one could infer quantitative

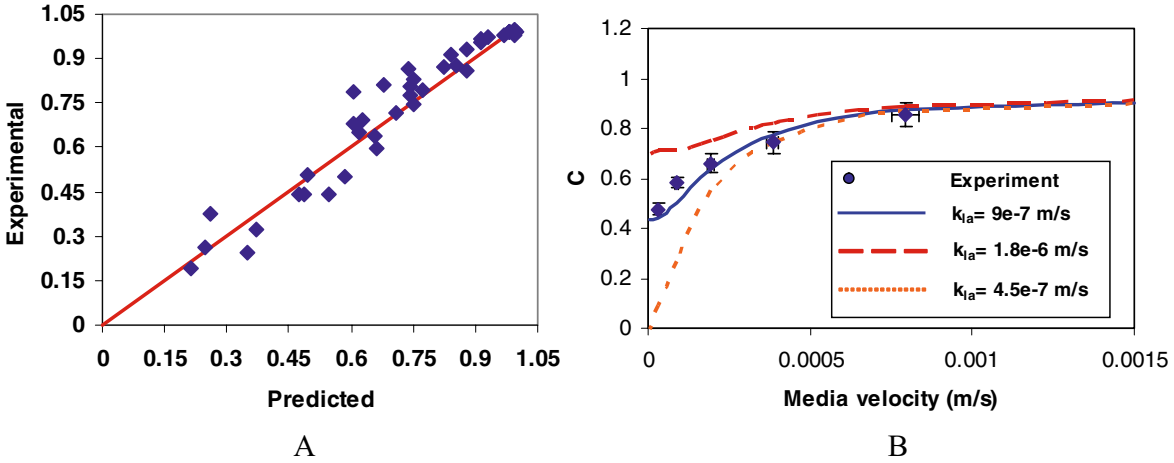

A B

Fig. 4 (A) Model predictions vs. Experimental data. The model predictions are compared with experimental data on the oxygen concentration at the outlet. The oxygen concentration is non-dimensionalized using the inlet oxygen concentrations. The line $y = x$ is shown as reference. The model was simulated based on the average values of cell density and operating flow rates as measured, with microbioreactor geometry parameters as described in Fig. 2. The parameters for uptake rates and mass transfer are: $V_{max} = 2.06\,\mathrm{e} - 16$, mol/cell/s, $K_m = 0.005$ mol/m^3, and $k_{la} = 9\mathrm{e} - 7$ m/s. B) Effect of diffusion of oxygen through PDMS on dimensionless outlet concentration, C. The value of mass-transfer coefficient k_{la} was varied to understand the contribution of oxygen diffusion from PDMS when $\phi = 5.12\mathrm{e}8$ cells/m^2. Solid line shows model prediction for $k_{la} = 9\mathrm{e} - 7$ m/s. Experimental data for the same conditions (solid circles) are shown as reference. The concentration is scaled with respect to the inlet concentration

information on the cellular oxygen uptake rates for wide variety of cell types.

3.5 Mathematical model and microfluidic PDMS bioreactor provide tools for spatio-temporal regulation of oxygen microenvironments

The results presented here demonstrate that we can understand and predict oxygen gradients in a perfused PDMS microfluidic bioreactor as a function of media flow rate and cell density. Significant axial (along the length of the bioreactor) gradients in oxygen concentration can exist for lower flow rates (low Pe/α), even with significant diffusion of oxygen through PDMS (high Sh). Axial concentration gradients also increase with increased cell density. These spatial gradients in oxygen concentrations could be a primary cause of spatial heterogeneity in cell density inside microfluidic bioreactors as observed in our previous experiments (Gu et al., 2004). Our modeling studies indicate that for a particular cell density the depletion in oxygen can be controlled by regulating flow velocity. Additionally, complementing perfusion with media recirculation would offer an additional means of lowering the concentration of oxygen inside the reactor to a desired level at all the stages of the cell culture. Modified channel geometries may also be used to engineer the concentration distribution of oxygen inside the reactor at desired levels (Mehta and Linderman, 2006).

The combined use of models together with experimental measurements and computerized fluid actuation enable powerful experimental systems in which cell responses to various oxygen gradients can be efficiently and systematically analyzed or an optimal oxygen environment can be dialed in for better cell function. When used at relatively slow flow rates and high cell density, this microbioreactor creates oxygen limited physiology (Duling, 1972; Pittman and Duling, 1975; Seiyama et al., 1996; Swain and Pittman, 1989; Tsai et al., 2003), which is known to be beneficial for a variety of applications, including maintaining the pluripotency of embryonic stem cells (Ezashi et al., 2005) and inducing the growth of erythroid colonies from bone marrow progenitors (Van Merris et al., 2001). Our device is capable of generating such conditions in ambient atmosphere without need of hypoxic chambers by simply taking advantage of cell respiration and the small volume of media in microfluidic systems. It has also been observed that even transient changes in oxygen levels can change gene transcription, thus affecting the fate of stem cells in culture conditions (Pfau et al., 2004). Our system provides convenient dynamic control of the oxygen environment by computer programmed temporal changes in the perfusion rates. Our experiments and analysis do indicate that manipulating the media flow rates is not always sufficient to achieve very low oxygen tensions inside the PDMS bioreactor. In order to obtain pathologic hypoxic conditions such as 0.01% oxygen (0.004 mg/l), alternative techniques would have to be used. We envision this biomedical microdevice to be useful in conducting key biological studies pertaining to the effect of physiologic oxygen microenvironments on cell behavior. In addition to the ability

to regulate oxygen microenvironments, this bioreactor reaps benefits of a typical PDMS device; including rapid prototyping, ease of fabrication, low cost, optical transparency, durability, disposability, and biological inertness.

4 Conclusion

We developed a method to measure dissolved oxygen content in real time in microfluidic PDMS perfusion systems using fluorescence intensity and lifetime imaging. Cell respiration created an axial oxygen gradient in the reactor along the length of a cell culture channel even though the device was mainly fabricated using highly gas-permeable PDMS. The downstream oxygen concentration decreased with increasing cell density and decreasing perfusion velocities. The measurements agree with a mathematical model which describes the spatial distribution of oxygen along the length of a microfluidic cell culture channel inside the bioreactor and enabled the estimation of oxygen transfer coefficients through the materials comprising our PDMS device.

These results are important not only for characterization of the specific device we describe in this report but also for formulating general guidelines for designing PDMS devices in regards to their oxygen microenvironment for mammalian cell culture. The relationship that describes the minimum convective flow rate that will offset specific oxygen consumption rates, as is described in this report, will be useful to the microfluidics community for designing devices and experimental conditions for microfluidic cell culture. In order to achieve oxygen gradients or hypoxic conditions in PDMS microbioreactors, researchers should plan experiments at low Sh, and low Pe/α. Our results also underscore the importance of characterizing the oxygen transfer rate of each type of PDMS device made under different conditions such as plasma oxidation and protein coating to explain cell behaviors observed as the oxygen permeability of a given device cannot always be predicted by simply using the permeability values of native bulk PDMS. The methods described here also provide an efficient method to perform such analyses.

Acknowledgments We thank Dr. Brian Johnson and Prof. Mark Burns, Department of Chemical Engineering, Univ. of Michigan for use of clean room facilities, Kenneth Chomistek, Department of Chemical Engineering, Univ. of Michigan for parylene coating on PDMS. This material is based upon work supported by the U.S. Army Research Laboratory and the U.S. Army Research Office under contract/grant number DAAD19-03-1-0168 and the National Science Foundation (BES-0238625).

References

J.W. Allen and S.N. Bhatia, Formation of steady-state oxygen gradients in vitro: application to liver zonation. Biotechnol. Bioeng. **82**, 253–262 (2003).

J.W. Allen, S.R. Khetani, and S.N. Bhatia, In vitro zonation and toxicity in a hepatocyte bioreactor. Toxicol. Sci. **84**: 110–119 (2005).

S. Andreescu, O.A. Sadik, D.W. McGee, and S. Suye, Autonomous multielectrode system for monitoring the interactions of isoflavonoids with lung cancer cells. Anal. Chem. **76**, 2321–2330 (2004).

R. Benninger, O. Hofmann, J. McGinty, J. Requejo-Isidro, I. Munro, M. Neil, A. deMello, and P. French, Time-resolved fluorescence imaging of solvent interactions in microfluidic devices. Opt. Express. **13**, 6275–6285 (2005).

D.A. Chang-Yen and B.K. Gale, An integrated optical oxygen sensor fabricated using rapid-prototyping techniques. Lab Chip. **3**, 297–301 (2003).

S.G. Charati and S.A. Stern, Diffusion of gases in silicone polymers: Molecular dynamics simulations. Macromol. **31**, 5529–5535 (1998).

M. Csete, Oxygen in the cultivation of stem cells. Ann. N. Y. Acad. Sci. **1049**, 1–8 (2005).

R.R. Deshpande and E. Heinzle, On-line oxygen uptake rate and culture viability measurement of animal cell culture using microplates with integrated oxygen sensors. Biotechnol. Lett. **26**, 763–767 (2004).

J.W. Dobrucki, Interaction of oxygen-sensitive luminescent probes Ru(phen)(3)(2+) and Ru(bipy)(3)(2+) with animal and plant cells in vitro. Mechanism of phototoxicity and conditions for non-invasive oxygen measurements. J. Photochem. Photobiol. B. **65**, 136–144 (2001).

D.C. Duffy, J.C. McDonald, Schueller OJA, and G.M. Whitesides, Rapid prototyping of microfluidic systems in poly(dimethylsiloxane). Anal. Chem. **70**, 4974–4984 (1998).

B.R. Duling, Microvascular responses to alterations in oxygen tension. Circ. Res. **31**, 481–489 (1972).

T. Ezashi, P. Das, and R.M. Roberts, Low O_2 tensions and the prevention of differentiation of hES cells. Proc. Natl. Acad. Sci. U S A **102**, 4783–4788 (2005).

R.J. Fleischaker and A.J. Sinskey, Oxygen demand and supply in cell culture. Appl. Microbiol. Biotechnol. **12**, 193 (1981).

N. Futai, W. Gu, and S. Takayama, Rapid prototyping of microstructures with bell-shaped cross-sections and its application to deformation-based microfluidic valves. Adv. Mater. **16**, 1320–1323 (2004).

N. Futai, W. Gu, J.W. Song, and S. Takayama, Handheld recirculation system and customized media for microfluidic cell culture. Lab Chip. **6**, 149–154 (2006).

H.C. Gerritsen, R. Sanders, A. Draaijer, and Y.K. Levine, Flourescence lifetime imaging of oxygen in living Cells. J. Flourescence. **7**, 11–16 (1997).

W. Gu, X. Zhu, N. Futai, B.S. Cho, and S. Takayama, Computerized microfluidic cell culture using elastomeric channels and Braille displays. Proc. Natl. Acad. Sci. USA **101**, 15861–15866 (2004).

Y.S. Heo, L.M. Cabrera, J.W. Song, N. Futai, Y-C Tung, G.D. Smith, and S. Takayama, Characterization and resolution of evaporation-mediated osmolality shifts that constrain microfluidic cell culture in poly(dimethylsiloxane) devices. Submitted to Anal. Chem. (2006).

E.Y. Hwang, D. Pappas, A.S. Jeevarajan, and M.M. Anderson, Evaluation of the paratrend multi-analyte sensor for potential utilization in long-duration automated cell culture monitoring. Biomed. Microdevices. **6**, 241–249 (2004).

G.T. John, I. Klimant, C. Wittmann, and E. Heinzle, Integrated optical sensing of dissolved oxygen in microtiter plates: a novel tool for microbial cultivation. Biotechnol. Bioeng. **81**, 829–836 (2003).

E. Leclerc, B. David, L. Griscom, B. Lepioufle, T. Fujii, P. Layrolle, and C. Legallaisa, Study of osteoblastic cells in a microfluidic environment. Biomaterials. **27**, 586–595 (2006).

E. Leclerc, Y. Sakai, and T. Fujii, Cell culture in 3-Dimensional microfluidic structure of PDMS (polydimethylsiloxane). Biomed. Microdevices. **5**, 109 (2003).

E. Leclerc, Y. Sakai, and T. Fujii, Microfluidic PDMS (polydimethylsiloxane) bioreactor for large-scale culture of hepatocytes. Biotechnol. Prog. **20**, 750–755 (2004).

J. Malda, J. Rouwkema, D.E. Martens, E.P. Le Comte, F.K. Kooy, J. Tramper, C.A. van Blitterswijk, and J. Riesle, Oxygen gradients in tissue-engineered PEGT/PBT cartilaginous constructs: measurement and modeling. Biotechnol. Bioeng. **86**, 9–18 (2004).

K. Mehta and J.J. Linderman, Model-based analysis and design of a microchannel reactor for tissue engineering. Biotechnol. Bioeng. **94**, 596–609 (2006).

T.C. Merkel, V.I. Bondar, K. Nagai, B.D. Freeman, and I. Pinnau, Gas sorption, diffusion, and permeation in poly(dimethylsiloxane). J. Polym. Sci. Part B-Polym. Phys. **38**, 415–434 (2000).

S.M. Mitrovski and R.G. Nuzzo, An electrochemically driven poly(dimethylsiloxane) microfluidic actuator: oxygen sensing and programmable flows and pH gradients. Lab Chip. **5**, 634–645 (2005).

G.F. Muschler, C. Nakamoto, and L.G. Griffith, Engineering principles of clinical cell-based tissue engineering. J. Bone Joint Surg. Am. **86-A**, 1541–1558 (2004).

J. Park, T. Bansal, M. Pinelis, and M.M. Maharbiz, A microsystem for sensing and patterning oxidative microgradients during cell culture. Lab Chip. **6**, 611–622 (2006).

T.H. Park and M.L. Shuler, Integration of cell culture and microfabrication technology. Biotechnol. Prog. **19**, 243–253 (2003).

J.C. Pfau, J.C. Schneider, A.J. Archer, J. Sentissi, F.J. Leyva, and J. Cramton, Environmental oxygen tension affects phenotype in cultured bone marrow-derived macrophages. Am. J. Physiol. Lung Cell. Mol. Physiol. **286**, L354–L362 (2004).

R.N. Pittman and B.R. Duling, Measurement of percent oxyhemoglobin in the microvasculature. J. Appl. Physiol. **38**, 321–327 (1975).

P. Roy, H. Baskaran, A.W. Tilles, M.L. Yarmush, and M. Toner, Analysis of oxygen transport to hepatocytes in a flat-plate microchannel bioreactor. Ann. Biomed. Eng. **29**, 947–955 (2001).

A. Seiyama, S. Tanaka, H. Kosaka, and T. Shiga, O2 transfer from single microvessels to acinar cells in secretin-stimulated pancreas of rat. Am. J. Physiol. **270**, H1704–H1711 (1996).

H. Shiku, T. Saito, C-C Wu, T. Yasukawa, M. Yokoo, H. Abe, T. Matsue, and H. Yamada, Oxygen permeability of surface-modified poly(dimethylsiloxane) characterized by scanning electrochemical microscopy. Chem. Lett. **35**, 234 (2006).

A. Sin, K.C. Chin, M.F. Jamil, Y. Kostov, G. Rao, and M.L. Shuler, The design and fabrication of three-chamber microscale cell culture analog devices with integrated dissolved oxygen sensors. Biotechnol. Prog. **20**, 338–345 (2004).

J.W. Song, W. Gu, N. Futai, K.A. Warner, J.E. Nor, and S. Takayama, Computer-controlled microcirculatory support system for endothelial cell culture and shearing. Anal. Chem. **77**, 3993–3999 (2005).

D. Sud, G. Mehta, K. Mehta, J. Linderman, S. Takayama, and M.-A. Mycek, Optical imaging in microfluidic bioreactors enables oxygen monitoring for continuous cell culture, J. Biomed. Opt. **11**(5), 050504 (Published on the web on Sep. 28) (2006a).

D. Sud, W. Zhong, D.G. Beer, and M.A. Mycek, Time-resolved optical imaging provides a molecular snapshot of altered metabolic function in living human cancer cell models. Opt. Express. **14**, 4412–4426 (2006b).

D.P. Swain and R.N. Pittman, Oxygen exchange in the microcirculation of hamster retractor muscle. Am. J. Physiol. **256**, H247–H255 (1989).

I.R. Sweet, G. Khalil, A.R. Wallen, M. Steedman, K.A. Schenkman, J.A. Reems, S.E. Kahn, and J.B. Callis, Continuous measurement of oxygen consumption by pancreatic islets. Diabetes Technol. Ther. **4**, 661–672 (2002).

N. Szita, P. Boccazzi, Z. Zhang, P. Boyle, A.J. Sinskey, and K.F. Jensen, Development of a multiplexed microbioreactor system for high-throughput bioprocessing. Lab Chip. **5**, 819–826 (2005).

L. Tolosa, Y. Kostov, P. Harms, and G. Rao, Noninvasive measurement of dissolved oxygen in shake flasks. Biotechnol. Bioeng. **80**, 594–597 (2002).

A.G. Tsai, P.C. Johnson, and M. Intaglietta, Oxygen gradients in the microcirculation. Physiol. Rev. **83**, 933–963 (2003).

P. Urayama, W. Zhong, J.A. Beamish, F.K. Minn, R.D. Sloboda, K.H. Dragnev, E. Dmitrovsky, and M.A. Mycek, A UV-Visible-NIR fluorescence lifetime imaging microscope for laser-based biological sensing with picosecond resolution. Appl. Phys. B: Lasers and Optics. **76**, 483 (2003).

V. Van Merris, M. Lenjou, D. Hoeben, G. Nijs, D. Van Bockstaele, and C. Burvenich, Culture of bovine bone marrow progenitor cells in vitro. Vet. Q. **23**, 170–175 (2001).

A.P. Vollmer, R.F. Probstein, R. Gilbert, and T. Thorsen, Development of an integrated microfluidic platform for dynamic oxygen sensing and delivery in a flowing medium. Lab Chip. **5**, 1059–1066 (2005).

G.M. Walker, M.S. Ozers, and D.J. Beebe, Insect cell culture in microfluidic channels. Biomed. Microdevices. **4**, 161 (2002).

Y.S. Yeh, W.J. James, and H. Yasuda, Polymerization of para-xylylene derivatives.6. Morphology of parylene-N and parylene-C films investigated by gas-transport characteristics. J. Polym. Sci. Part B-Polym. Phys. **28**, 545–568 (1990).

Z. Yun, Q. Lin, and A.J. Giaccia, Adaptive myogenesis under hypoxia. Mol. Cell. Biol. **25**, 3040–3055 (2005).

A. Zanzotto, N. Szita, P. Boccazzi, P. Lessard, A.J. Sinskey, and K.F. Jensen, Membrane-aerated microbioreactor for high-throughput bioprocessing. Biotechnol. Bioeng. 87, 243–254 (2004).

W. Zhong, P. Urayama, M-A Mycek, Imaging fluorescence lifetime modulation of a ruthenium-based dye in living cells: the potential for oxygen sensing. J. Phys. D: Appl. Phys. **36**, 1689 (2003).